magnetochemistry

MDPI

Article

Field-Induced Single-Ion Magnet Phenomenon in Hexabromo- and Hexaiodorhenate(IV) Complexes

Carlos Rojas-Dotti [1,2], Adrián Sanchis-Perucho [1], Marta Orts-Arroyo [1], Nicolás Moliner [1], Ricardo González [2,*], Francesc Lloret [1] and José Martínez-Lillo [1,*]

[1] Instituto de Ciencia Molecular (ICMol)/Departament de Química Inorgànica, Universitat de València, c/Catedrático José Beltrán 2, 46980 Paterna, Valencia, Spain; carlos.rojas@uv.es (C.R.-D.); adrian.sanchis@uv.es (A.S.-P.); marta.orts-arroyo@uv.es (M.O.-A.); fernando.moliner@uv.es (N.M.); francisco.lloret@uv.es (F.L.)

[2] Cátedra de Química Inorgánica, Departamento Estrella Campos, Facultad de Química, Universidad de la República, Avda. General Flores 2124, Montevideo CC 1157, Uruguay

* Correspondence: rgonzale@fq.edu.uy (R.G.); f.jose.martinez@uv.es (J.M.-L.)

Received: 4 April 2020; Accepted: 17 April 2020; Published: 22 April 2020

Abstract: Two mononuclear Re^{IV} complexes of general formula $(PPh_4)_2[ReX_6]$ [PPh_4^+ = tetraphenylphosphonium cation, X = Br (**1**) and I (**2**)] have been prepared and structurally and magnetically characterised. Both compounds crystallise in the triclinic system with space group $P\bar{1}$. Their structures are made up of hexahalorhenate(IV), $[ReX_6]^{2-}$, anions, and bulky PPh_4^+ cations. Each Re^{IV} ion in **1** and **2** is six-coordinate and bonded to six halide ions in a quasi regular octahedral geometry. In their crystal packing, the $[ReX_6]^{2-}$ anions are well separated from each other through the organic cations, generating alternated anionic and cationic layers, and no intermolecular Re−X···X−Re interactions are present. Variable-temperature dc magnetic susceptibility measurements performed on microcrystalline samples of **1** and **2** show a very similar magnetic behaviour, which is typical of noninteracting mononuclear Re^{IV} complexes with $S = 3/2$. Ac magnetic susceptibility measurements reveal the slow relaxation of the magnetisation in the presence of external dc fields for **1** and **2**, hence indicating the occurrence of the field-induced single-ion magnet (SIM) phenomenon in these hexabromo- and hexaiodorhenate(IV) complexes.

Keywords: rhenium; crystal structures; AC/DC measurements; molecular magnetism; single-ion magnets

1. Introduction

The last decade has witnessed a rapid advance in the development of mononuclear Single-Molecule Magnets (SMMs), the so-called Single-Ion Magnets (SIMs), which are mainly discrete molecules that are based on one paramagnetic and highly anisotropic ion belonging mainly to the d-block or f-block metals and displaying slow relaxation of the magnetisation [1–14]. These nanosized magnetic systems are often considered to be promising candidates for future technological applications, such as high-density information storage or quantum computing at the molecular level, among others [15,16].

In comparison, SIMs containing 4d/5d metal ions have been far less investigated than their 3d-based analogues [17–19]. Indeed, the first SIMs based on a 5d metal ion, namely, the $(NBu_4)_2[ReX_4(ox)]$ systems (X = Cl and Br; ox = oxalate anion), were published by some of us in 2013 [20]. Just one year later, Pedersen et al. reported the research work that deals with the study of the $(PPh_4)_2[ReF_6]\cdot 2H_2O$ compound [21]. Afterwards, the photoluminescent $(Th_2imH)_2[ReCl_6]$ complex (Th_2imH = protonated bisthienylethene) and the $(NBu_4)_2[ReCl_4(CN)_2]\cdot 2DMA$ (DMA = *N*,*N*-dimethylacetamide) compound, that as the previously reported 5d-SIMs display field-induced slow magnetic relaxation, were also studied and published [22,23]. These last systems complete the short list of SIMs that are based on the

highly anisotropic Re^{IV} metal ion. Recently, additional 5d-SIMs containing the Os^{V} and Ir^{IV} metal ions have also been reported [24–26].

We have studied further hexahalorhenate(IV) salts of the PPh_4^+ cation to develop our investigation in 5d-SIMs. Thus, by means of this bulky cation, the well-known intermolecular Re-X···X-Re (X = halide ion) interactions, with pathways that can mediate significant magnetic exchanges between neighbouring $[ReX_6]^{2-}$ complexes in the crystal lattice, hence annulling the SIM behaviour of such systems, are avoided [18,27–42].

Herein, we report the preparation, crystal structures, and magnetic properties of two mononuclear Re^{IV} complexes of general formula $(PPh_4)_2[ReX_6]$ [PPh_4^+ = tetraphenylphosphonium cation, X = Br (**1**) and I (**2**)], moreover studying the effect of the halide ligand and the crystal packing on the magnetisation relaxation dynamics.

2. Results and Discussion

2.1. Description of the Crystal Structures

The two compounds (**1** and **2**) crystallise in the triclinic system with space group $P\bar{1}$ (Table 1). Their structures are made up of hexahalorhenate(IV) $[ReX_6]^{2-}$ [X = Br (**1**) and I (**2**)] anions and bulky PPh_4^+ cations, which are mainly held by electrostatic forces along with weak intermolecular X···H-C and X···π interactions. In their asymmetric unit, fragments of $[ReX_6]^{2-}$ anions and entire PPh_4^+ cations are present (Figure 1).

Table 1. Summary of the crystal data and structure refinement parameters for **1** and **2**.

Compound	1	2
CCDC	1956543	1956544
Formula	$C_{48}H_{40}P_2Br_6Re$	$C_{48}H_{40}P_2I_6Re$
M_r/g mol^{-1}	1344.40	6505.35
Crystal system	Triclinic	Triclinic
Space group	$P\bar{1}$	$P\bar{1}$
a/Å	10.319(1)	17.370(1)
b/Å	10.434(1)	18.058(1)
c/Å	12.082(1)	18.475(1)
α/°	92.66(1)	108.52(1)
β/°	99.89(1)	105.58(1)
γ/°	117.12(1)	100.23(1)
V/Å^3	1129.1(1)	5069.5(6)
Z	1	1
D_c/g cm^{-3}	1.977	2.131
μ(Mo-K$_\alpha$)/mm^{-1}	8.104	6.145
F(000)	643	3004
Goodness-of-fit on F^2	1.031	1.201
R_1 [$I > 2\sigma(I)$]	0.0351	0.0466
wR_2 [$I > 2\sigma(I)$]	0.0651	0.1422

In **1** and **2**, each Re^{IV} ion is six-coordinate and bonded to six halide ions in a quasi regular octahedral geometry. The Re-X bond lengths vary in the ranges of 2.498(1)–2.526(1) Å and 2.710(1)–2.746(1) Å for **1** and **2**, respectively. The values of the X(1)-Re-X(2) and X(2)-Re-X(3) angles cover the ranges of 90.1(1)–91.6(1)° (**1**) and 88.3(1)–91.7(1)° (**2**). These structural data are in agreement with those that were previously reported for salts containing the anionic $[ReX_6]^{2-}$ units [27–39]. The PPh_4^+ cations in **1** and **2** counterbalance the negative charges and show values of C-C and C-P bond lengths typical of the phenyl groups linked to the central phosphorous atom.

In the crystal packing of **1** and **2**, the $[ReX_6]^{2-}$ anions are well separated from each other through the bulky PPh_4^+ cations, which generate alternated anionic and cationic layers, respectively (Figure 2a,b). The shortest Re···Re separation is ca. 10.43 (**1**) and 10.85 Å (**2**). The shortest X···X distance

is approximately 6.52 and 5.93 Å for **1** and **2**, respectively. It is worth pointing out that the $[ReBr_6]^{2-}$ anions are arranged in a very similar way in **1**, that is, with all of the anionic units orientated in the same direction, whereas the $[ReI_6]^{2-}$ anions display different orientations in the crystal of **2** (Figure 2).

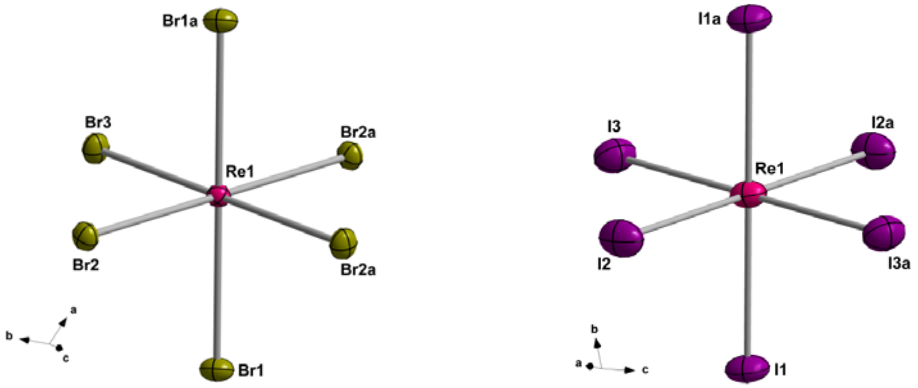

(**a**) (**b**)

Figure 1. Perspective view of the $[ReBr_6]^{2-}$ and $[ReI_6]^{2-}$ anions of the compounds **1** (**a**) and **2** (**b**). The PPh_4^+ cations have been omitted for clarity. The thermal ellipsoids are depicted at the 50% probability level.

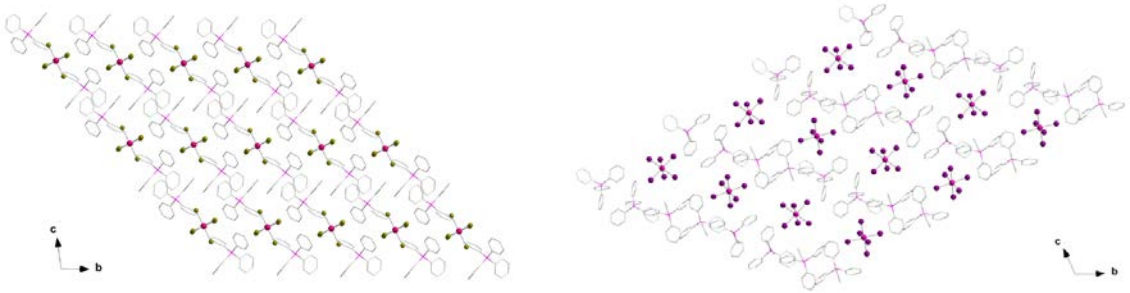

(**a**) (**b**)

Figure 2. View along the crystallographic *a* axis of a fragment of the crystal packing of **1** (**a**) and **2** (**b**) showing the arrangement of the $[ReX_6]^{2-}$ anions (ball and stick model) and PPh_4^+ cations (wireframe model).

The PPh_4^+ cations in both of the compounds show several intermolecular phenyl–phenyl interactions that provide noticeable supramolecular conformations. Indeed, the sextuple phenyl embrace (SPE) supramolecular conformation is present in both **1** and **2** (Figure S1) [43–45]. The shortest P···P distance between PPh_4^+ cations displaying the SPE conformation is ca. 6.07 and 6.13 Å for **1** and **2**, respectively. Additionally, weak intermolecular X···H-C (the shortest X···C distance being 3.66 (**1**) and 3.85 Å (**2**)) and X···π (halide-centroid distance of 3.66 (**1**) and 4.4 Å (**2**)) interactions between anions and cations contribute to stabilizing the crystal structure of the two compounds.

2.2. *Magnetic Properties*

2.2.1. Dc Magnetic Susceptibility

The magnetic properties of the reported compounds were studied through direct current (dc) magnetic susceptibility measurements, which were performed on the microcrystalline samples of **1** and **2** in the 2–300 K temperature range and under an external magnetic dc field of 0.5 T. Powder XRD previously confirmed the purity and homogeneity of these bulk samples (Figure S2). Both of the compounds exhibit a very similar behaviour that is represented in the form of $\chi_M T$ *versus* T plots (χ_M being the molar magnetic susceptibility per Re^{IV} ion) for **1** and **2** in Figure 3. At room temperature,

the $\chi_M T$ values are approximately 1.58 (**1**) and 1.54 $cm^3mol^{-1}K$ (**2**), which fall into the range that was reported for systems containing a magnetically isolated Re^{IV} (S = 3/2 with g = 1.80–1.90) metal ion [18,27–42]. Upon cooling, the $\chi_M T$ values for these compounds decrease first slowly and, around 70–80 K, they decrease faster, reaching minimum values of approximately 0.95 (**1**) and 0.96 $cm^3mol^{-1}K$ (**2**) at 2.0 K. These minimum values obtained at very low temperature are close to that expected for a magnetically isolated Re^{IV} ion (*ca.* 1.0 $cm^3mol^{-1}K$), as previously reported [18]. The decrease of the $\chi_M T$ values observed for complexes **1** and **2** is mainly due to zero-field splitting (ZFS) effects, which are very significant in Re^{IV}-based systems [18,27–42].

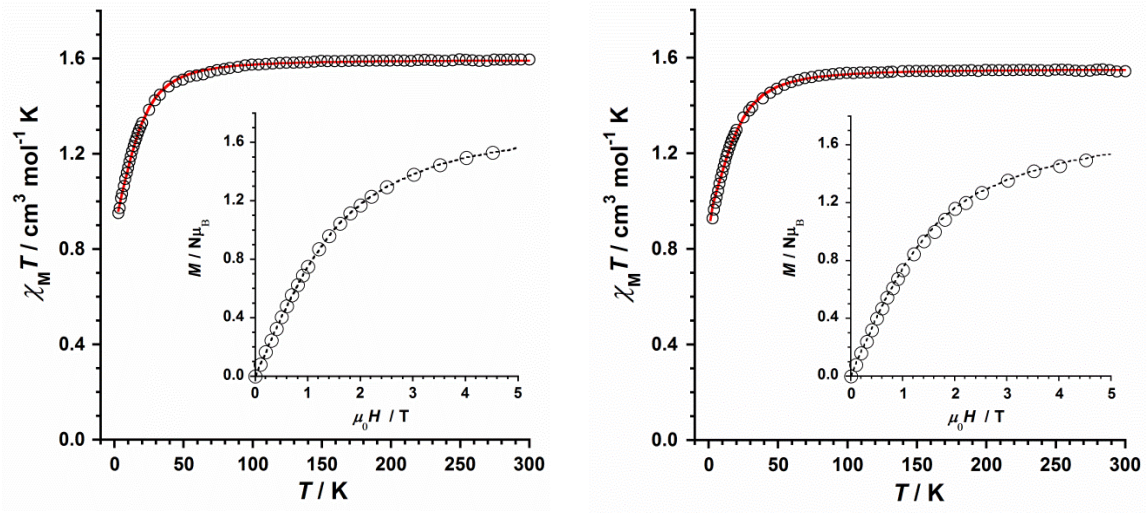

Figure 3. Thermal variation of the $\chi_M T$ product for **1** (**a**) and **2** (**b**). The solid red line represents the theoretical fit of the experimental data and the inset shows the *M versus H* plot at 2.0 K obtained for **1** and **2**, the dashed line being a guide to the eye.

A field dependence of the molar magnetisation (M) plot for **1** and **2** at 2.0 K is given in the respective insets of Figure 3a(**1**),b(**2**). In all the cases, the M values display a continuous increase with the applied magnetic field, the higher M values being 1.57 (**1**) and 1.53 μ_B (**2**) at 5.0 T, which are in agreement with those of similar mononuclear Re^{IV} complexes that were reported in the literature [18,27–41]. Given that no significant intermolecular interactions are observed in the crystal structures of **1** and **2**, as indicated in the structure description, the shortest intermolecular Re-X···X-Re distances are covering the range of 5.93–6.52 Å, we have performed the treatment of the experimental data of the $\chi_M T$ *versus* T plots through the anisotropic Hamiltonian of Equation (1) (where $\hat{S}_z$ is the easy-axis spin operator, H is the applied field, β is the Bohr magneton, g is the Landé factor, and D is the ZFS for the Re^{IV} ion).

$$\hat{H} = D[(\hat{S}_Z)^2 - S(S+1)/3] + g_{//}\beta H_Z \hat{S}_Z + g_\perp \beta (H_X \hat{S}_X + H_Y \hat{S}_Y) \quad (1)$$

By assuming that $g_{\|} = g_\perp = g$ for the two complexes, we have fitted the experimental magnetic susceptibility data of the compounds **1** and **2**, affording the following parameters: $|D|$ = 22.0(2) cm^{-1}, g = 1.84(2) with $R = 5.6 \times 10^{-5}$ for **1** and $|D|$ = 24.0(2) cm^{-1}, g = 1.82(2) with $R = 2.4 \times 10^{-5}$ for **2** (R being the agreement factor defined as $\Sigma_i[(\chi_M T)_i^{obs} - (\chi_M T)_i^{calc}]^2/[(\chi_M T)_i^{obs}]^2$). The solid red line, indicating the fit in Figure 3a(**1**),b(**2**), matches quite well the experimental curves in both cases. The g and D values that are computed for **1** and **2** are in agreement with those calculated for previously reported mononuclear Re^{IV} complexes [18,27–41]. The $|D|$ value that is obtained for **2** is somewhat greater than that of the complex **1**.

2.2.2. Ac Magnetic Susceptibility

Alternating current (ac) magnetic susceptibility measurements were performed on microcrystalline samples of **1** and **2** in the temperature range of 2–7 K and in a 3.5 G ac field oscillating at different frequencies. In both cases, no out-of-phase ac signals (χ''_M) are observed at H_{dc} = 0 G. However, out-of-phase ac signals, with observable χ''_M maxima, take place at low temperatures in **1** and **2** when an external dc magnetic field (H_{dc} = 1000 and 5000 G) is applied (Figures 4 and 5). This magnetic behaviour would indicate that the two studied systems (**1** and **2**) exhibit slow relaxation of the magnetisation and, therefore, single-ion magnet (SIM) phenomenon [1–21]. Nevertheless, the relaxation dynamics that the two compounds exhibit is not equally affected by the external dc magnetic fields. While the H_{dc} = 5000 G seems to be optimal for compound **1** (with the presence of more χ''_M maxima that shift towards higher frequencies), this magnetic field results in being less useful for studying the magnetic relaxation in **2**, where a decrease of the number of χ''_M maxima in the χ''_M versus ν plot occurs (Figures 4 and 5). In both **1** and **2**, the intensity of the χ''_M peaks increases with increasing the external dc magnetic field.

The insets in Figures 4 and 5 show the ln(τ) versus 1/T plot for complexes **1** and **2**, respectively. In the high-temperature region, the experimental data that were obtained from the frequency-dependent χ''_M peaks draw a straight line pretty much in both cases along the ranges of ca. 0.25–0.35 K^{-1} for **1** ca. 0.35–0.50 K^{-1} for **2**. Consequently, these experimental data were fitted to the Arrhenius equation ($\tau = \tau_o \exp(U_{eff}/k_BT)$, where τ_o is the preexponential factor, τ is the relaxation time, U_{eff} is the anisotropy (effective) energy barrier to the magnetisation reorientation, and k_B is the Boltzmann constant) by considering that the magnetisation relaxation only involves an Orbach process [12]. In this way, we can evaluate the U_{eff} and τ_o parameters in this region for **1** and **2** and compare their values with those previously reported. These fits are indicated as dashed lines in the insets of Figures 4 and 5, and Table 2 provides the U_{eff} and τ_o values thus obtained for **1** and **2**.

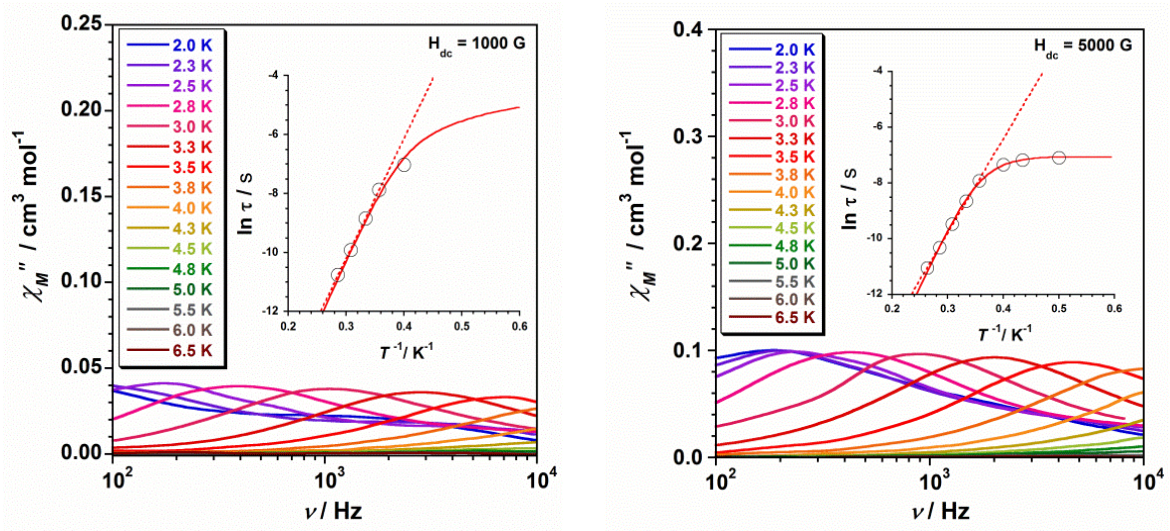

Figure 4. Frequency dependence of the out-of-phase ac susceptibility signals under dc fields of 1000 (**a**) and 5000 G (**b**) for compound **1**. The respective inset shows the ln(τ) *versus* 1/T plot for **1** with the fit to the Arrhenius law (dashed line) and the fit considering several mechanisms (solid line).

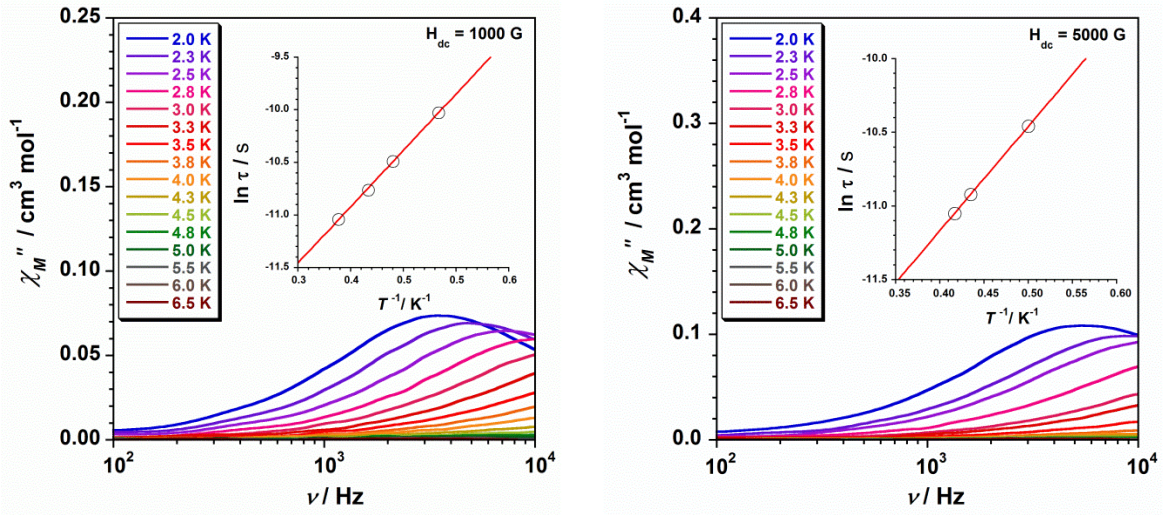

Figure 5. Frequency dependence of the out-of-phase ac susceptibility signals under dc fields of 1000 (**a**) and 5000 G (**b**) for compound **2**. The respective inset shows the ln(τ) *versus* 1/T plot for **2** with the fit performed through the Arrhenius law (solid line) corresponding to the Orbach mechanism.

Table 2. U_{eff} and τ_o values obtained through the dc applied magnetic fields of 1000 and 5000 G and the Arrhenius law for **1** and **2**.

Compound	H_{dc}/G	U_{eff}/K	τ_o/s
1	1000	40.6	1.89×10^{-10}
	5000	33.7	2.28×10^{-9}
2	1000	7.2	1.24×10^{-6}
	5000	7.0	8.38×10^{-7}

The U_{eff} values for **1** are similar between them at both 1000 and 5000 G, and much higher (approximately five/six times) than that of compound **2** (Table 2). Besides, the energy barrier value of **2** remains practically unaffected with increasing the dc applied magnetic field. The τ_o parameter for **1** and **2** shows values that are in agreement with those that were reported for similar Re^{IV} complexes displaying SIM behaviour [20–23].

In the low-temperature region of the ln(τ) versus 1/T plots, curved lines are only observed for **1**, which are better defined when the H_{dc} = 5000 G is applied (Figures 4 and 5). These features would account for the occurrence in such conditions of several relaxation processes, especially in compound **1**. In consequence, the whole experimental curve from these ln(τ) versus 1/T plots was fitted through Equation (2), where four mechanisms for spin-lattice relaxation of magnetisation can be considered, namely, Orbach ($\tau_o{}^{-1}\exp(-U_{eff}/k_BT)$), direct (AT), Raman ($CT^n$), and Quantum Tunnelling (QTM) [12].

$$\tau^{-1} = \tau^{-1}_{ORBACH} + \tau^{-1}_{DIRECT} + \tau^{-1}_{RAMAN} + \tau^{-1}_{QTM} \quad (2)$$

All the four mechanisms were considered during the fitting process of the ln(τ) versus 1/T curve for **1** that was obtained at the optimal magnetic field of 5000 G, whereas in the case of the treatment of the experimental data acquired with H_{dc} = 1000 G, the fourth term (QTM) was kept equal to zero (Table 3). The least-squares fit of the experimental data of **1** through Equation (2) leads to the set of parameters listed in Table 3. From these results, it is worthy to point out that the U_{eff} values thus obtained for compound **1** are somewhat higher than those calculated through the Arrhenius law and listed in Table 2. Besides, the U_{eff} parameter for **1** remains higher than that of **2**. Indeed, the effective energy barrier value obtained at the optimal dc field (H_{dc} = 5000 G) for **1** [43.3 K (30.1 cm^{-1})] is even

larger than those previously reported for the hexahalo $(PPh_4)_2[ReF_6]\cdot 2H_2O$ and $(Th_2imH)_2[ReCl_6]$ compounds [21,22]. The computed values of τ_o and τ_{QTM} for **1** agree with those that were reported for other 5d-SIMs [20–23]. On the other hand, the n values for **1** lie between 4.3 and 5.5 and fall into the range typical of metal ions with relaxation through optical and acoustic Raman-like process (n being equal to 9 for the Raman relaxation of Kramer ions) [12]. These n values are very close to those that were obtained for similar 5d-SIMs (Table 3) [24–26].

Table 3. Parameters of the magnetic relaxation obtained through the dc applied magnetic fields of 1000 and 5000 G and the Equation (2) for **1**.

H_{dc}/G	U_{eff}/K	τ_o/s	$A/s^{-1}K^{-1}$	$C/s^{-1}K^{-n}$	n	τ_{QTM}/s
1000	43.8	6.9×10^{-11}	69.9	2.5	5.5	-
5000	43.3	1.7×10^{-10}	743.1	19.7	4.3	4.4×10^{-4}

The frequency-dependent ac magnetic susceptibility data of compounds **1** and **2** were modelled to give the Cole-Cole plots that are shown in Figure 6. The obtained values for the α parameter are in the ranges of 0.09–0.17 (**1**) and 0.06–0.11 (**2**), with these values suggesting a narrow distribution of the relaxation times for these mononuclear Re^{IV} complexes [20–25].

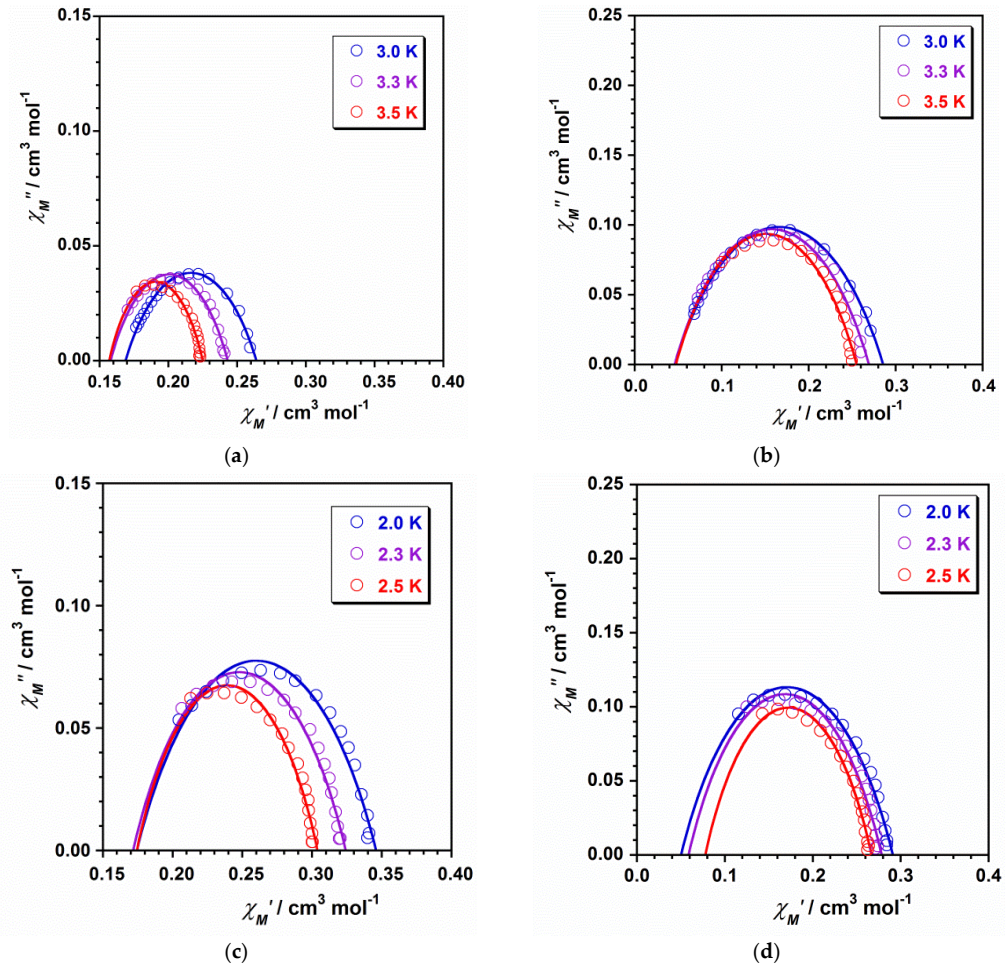

Figure 6. Cole–Cole plots for **1** (**a**,**b**) and **2** (**c**,**d**) obtained from the experimental data of the out-of-phase ac susceptibility signals under dc fields of 1000 (**a**–**c**) and 5000 G (**b**–**d**).

3. Materials and Methods

3.1. Reagents and Instruments

All of the manipulations were performed under aerobic conditions, using materials as received (reagent grade). The Re^{IV} precursors, namely, the K_2ReBr_6 and K_2ReI_6 salts, were prepared following the synthetic methods described in the literature [29,30].

Elemental analyses (C, H, N) were performed by the Central Service for the Support to Experimental Research (SCSIE) at the University of Valencia. Infrared spectra of **1** and **2** were recorded with a PerkinElmer Spectrum 65 FT-IR spectrometer in the 4000–400 cm^{-1} region. The powder X-ray diffraction (PXRD) patterns of **1** and **2** confirmed the homogeneity of their bulk samples (Figure S2). Variable-temperature, solid-state direct current (dc) magnetic susceptibility data down to 2.0 K were collected on a Quantum Design MPMS-XL SQUID magnetometer that was equipped with a 5 T dc magnet. Experimental magnetic data were corrected for the diamagnetic contributions of the involved atoms by using Pascal's constants [46].

3.2. Preparation of the Compounds

3.2.1. Synthesis of $(PPh_4)_2[ReBr_6]$ (1)

PPh_4Br (41.9 mg, 0.1 mmol) was dissolved in a 1.0 M HBr solution (5.0 mL) and slowly added to a solution of K_2ReBr_6 (37.2 mg, 0.05 mmol) dissolved in a 1.0 M HBr solution (25.0 mL). The thus generated yellow solid was filtered off and then washed with cold isopropanol and diethyl ether. Orange crystals of **1** were grown in a MeCN:isopropanol (1:2, 20.0 mL, *v*/*v*) mixture. Yield: ca. 92.0%. Anal. Calcd. for $C_{48}H_{40}P_2Br_6Re$ (**1**): C, 42.88 and H, 3.00. Found: C, 43.02 and H, 2.96. IR peaks (KBr pellets, ν/cm^{-1}): 3055(m), 1584(m), 1482(m), 1439(s), 1107(s), 996(m), 722(vs), 690(s), and 529(vs).

3.2.2. Synthesis of $(PPh_4)_2[ReI_6]$ (2)

The synthesis of **2** was very similar to that of **1**. PPh_4I (46.6 mg, 0.1 mmol) was dissolved in a 1.0 M HI solution (5.0 mL) and slowly added to a solution of K_2ReI_6 (0.30 mg, 0.05 mmol) that was dissolved in a 1.0 M HI solution (25.0 mL). A brown solid was formed, which was filtered off and washed with cold isopropanol and diethyl ether. Dark-purple crystals of **2** were grown in a $CH_3CN:CH_2Cl_2$ (1:1, 30.0 mL, *v*/*v*) mixture. Yield: ca. 80.0%. Anal. Calcd. for $C_{48}H_{40}P_2I_6Re$ (**2**): C, 35.45 and H, 2.48. Found: C, 35.53 and H, 2.42. IR peaks (KBr pellets, ν/cm^{-1}): 3051(m), 1584(m), 1482(m), 1435(s), 1107(s), 996(m), 722(vs), 689(s), and 526(vs).

3.3. X-ray Data Collection and Structure Refinement

X-ray diffraction data from single crystals of dimensions 0.28 × 0.26 × 0.20 (**1**) and 0.18 × 0.13 × 0.08 mm^3 (**2**) were collected on a Bruker D8 Venture diffractometer with graphite-monochromated Mo-K_α radiation (λ = 0.71073 Å). Crystal parameters and refinement results for **1** and **2** are summarized in Table 1. The data were processed through SAINT [47] reduction and SADABS [48] multi-scan absorption software. The structure was solved with the SHELXS structure solution program through the Patterson method. The model was refined with version 2013/4 of SHELXL against F^2 on all data by full-matrix least squares [49–51]. In the two samples, all non-hydrogen atoms were anisotropically refined. All of the hydrogen atoms of the PPh_4^+ cations were set in calculated positions and refined isotropically by using the riding model. The graphical manipulations were performed with the DIAMOND program [52]. The CCDC codes are 1956543 and 1956544 for **1** and **2**, respectively.

4. Conclusions

In summary, the X-ray structures and magnetic properties of two mononuclear Re^{IV} complexes, of general formula $(PPh_4)_2[ReX_6]$ [PPh_4^+ = tetraphenylphosphonium cation, X = Br (**1**) and I (**2**)], have been reported. In their crystal lattices, the paramagnetic $[ReX_6]^{2-}$ anions are well separated

from each other by means of the bulky PPh_4^+ cations and no significant intermolecular Re−X···X−Re interactions are present. The study of the relaxation dynamics reveals that **1** and **2** are not equally affected by the external dc magnetic fields, the bromo-derivative complex **1** exhibiting the higher value of the energy barrier (U_{eff}) for the reverse of the magnetisation in this family of hexahalo $[ReX_6]^{2-}$ compounds. Indeed, the U_{eff} value for **1** is higher than those previously reported for Re^{IV}-based SIMs. Hence, the information generated by these results could be very useful in designing future magnetic materials that are based on Re^{IV} SIMs.

Supplementary Materials: The following are available online at http://www.mdpi.com/2312-7481/6/2/20/s1, Figure S1: Sextuple phenyl embrace (SPE) supramolecular conformation of the PPh_4^+ cations, Figure S2: Plots of the theoretical and experimental XRD patterns profile.

Author Contributions: Conceptualization, R.G. and J.M.-L.; funding acquisition, R.G., F.L. and J.M.-L.; methodology, C.R.-D.; A.S.-P.; M.O.-A.; N.M. and J.M.-L.; investigation, C.R.-D.; A.S.-P.; M.O.-A.; N.M.; F.L. and J.M.-L.; formal analysis, C.R.-D.; A.S.-P.; M.O.-A.; N.M. and J.M.-L.; writing-original draft preparation, R.G. and J.M.-L.; writing-review and editing, R.G. and J.M.-L. All authors have read and agreed to the published version of the manuscript.

Funding: This research was funded by the Ministerio de Ciencia e Innovación (Spain, grant numbers MDM-2015-0538 and CTQ2016-75068P) and the Agencia Nacional de Investigación e Innovación (Uruguay, grant number FCE-1-2017-1-136539).

Acknowledgments: A.S.-P., M.O.-A. and J.M.-L. thank the Spanish "FPU fellowships", "FPI fellowships" and "Ramón y Cajal" Programmes, respectively.

Conflicts of Interest: The authors declare no conflict of interest.

References

1. Craig, G.A.; Murrie, M. 3d single-ion magnets. *Chem. Soc. Rev.* **2015**, *44*, 2135–2147.
2. Frost, J.M.; Harrimana, K.L.M.; Murugesu, M. The rise of 3-d single-ion magnets in molecular magnetism: Towards materials from molecules? *Chem. Sci.* **2016**, *7*, 2470–2491.
3. Colacio, E.; Ruiz, J.; Ruiz, E.; Cremades, E.; Krzystek, J.; Carretta, S.; Cano, J.; Guidi, T.; Wernsdorfer, W.; Brechin, E.K. Slow Magnetic Relaxation in a Co^{II}–Y^{III} Single-Ion Magnet with Positive Axial Zero-Field Splitting. *Angew. Chem. Int. Ed.* **2013**, *52*, 9130–9134.
4. Vallejo, J.; Pascual-Álvarez, A.; Cano, J.; Castro, I.; Julve, M.; Lloret, F.; Krzystek, J.; De Munno, G.; Armentano, D.; Wernsdorfer, W.; et al. Field-induced hysteresis and quantum tunneling of the magnetization in a mononuclear manganese(III) complex. *Angew. Chem. Int. Ed.* **2013**, *52*, 14075–14079.
5. Zadrozny, J.M.; Xiao, D.J.; Atanasov, M.; Long, G.J.; Grandjean, F.; Neese, F.; Long, J.R. Magnetic blocking in a linear iron(I) complex. *Nat. Chem.* **2013**, *5*, 577–581.
6. Rechkemmer, Y.; Breitgoff, F.D.; van der Meer, M.; Atanasov, M.; Hakl, M.; Orlita, M.; Neugebauer, P.; Neese, F.; Sarkar, B.; van Slageren, J. A four-coordinate cobalt(II) single-ion magnet with coercivity and a very high energy barrier. *Nat. Commun.* **2016**, *7*, 10467.
7. Atzori, M.; Tesi, L.; Benci, S.; Lunghi, A.; Righini, R.; Taschin, A.; Torre, R.; Sorace, L.; Sessoli, R. Quantum Coherence Times Enhancement in Vanadium(IV)-based Potential Molecular Qubits: The Key Role of the Vanadyl Moiety. *J. Am. Chem. Soc.* **2017**, *139*, 4338–4341.
8. Liu, J.; Chen, Y.-C.; Liu, J.-L.; Vieru, V.; Ungur, L.; Jia, J.-H.; Chibotaru, L.F.; Lan, Y.; Wernsdorfer, W.; Gao, S.; et al. A Stable Pentagonal Bipyramidal Dy(III) Single-Ion Magnet with a Record Magnetization Reversal Barrier over 1000 K. *J. Am. Chem. Soc.* **2016**, *138*, 5441–5450.
9. Guo, F.-S.; Day, B.M.; Chen, Y.-C.; Tong, M.-L.; Mansikkamäki, A.; Layfield, R.A. A Dysprosium Metallocene Single-Molecule Magnet Functioning at the Axial Limit. *Angew. Chem. Int. Ed.* **2017**, *56*, 11445–11449.
10. Goodwin, C.A.P.; Ortu, F.; Reta, D.; Chilton, N.F.; Mills, D.P. Molecular magnetic hysteresis at 60 kelvin in dysprosocenium. *Nature* **2017**, *548*, 439–442.
11. Guo, F.-S.; Day, B.M.; Chen, Y.-C.; Tong, M.-L.; Mansikkamäk, A.; Layfield, R.A. Magnetic hysteresis up to 80 kelvin in a dysprosium metallocene single-molecule magnet. *Science* **2018**, *362*, 1400–1403.
12. McAdams, S.G.; Ariciu, A.-M.; Kostopoulos, A.K.; Walsh, J.P.S.; Tuna, F. Molecular single-ion magnets based on lanthanides and actinides: Design considerations and new advances in the context of quantum technologies. *Coord. Chem. Rev.* **2017**, *346*, 216–239.

13. Canaj, A.B.; Dey, S.; Regincós Martí, E.; Wilson, C.; Rajaraman, G.; Murrie, M. Insight into D_{6h} Symmetry: Targeting Strong Axiality in Stable Dysprosium(III) Hexagonal Bipyramidal Single-Ion Magnets. *Angew. Chem. Int. Ed.* **2019**, *58*, 1–7.
14. Escalera-Moreno, L.; Baldoví, J.J.; Gaita-Ariño, A.; Coronado, E. Exploring the High-Temperature Frontier in Molecular Nanomagnets: From Lanthanides to Actinides. *Inorg. Chem.* **2019**, *58*, 11883–11892.
15. Miller, J.S.; Gatteschi, D. Molecule-based magnets. *Chem. Soc. Rev.* **2011**, *40*, 3065–3066.
16. Troiani, F.; Affronte, M. Molecular spins for quantum information technologies. *Chem. Soc. Rev.* **2011**, *40*, 3119–3129.
17. Wang, X.-Y.; Avendaño, C.; Dunbar, K.R. Molecular magnetic materials based on 4d and 5d transition metals. *Chem. Soc. Rev.* **2011**, *40*, 3213–3238.
18. Martínez-Lillo, J.; Faus, J.; Lloret, F.; Julve, J. Towards multifunctional magnetic systems through molecular-programmed self assembly of Re(IV) metalloligands. *Coord. Chem. Rev.* **2015**, *289*, 215–237.
19. Ferrando-Soria, J.; Vallejo, J.; Castellano, M.; Martínez-Lillo, J.; Pardo, E.; Cano, J.; Castro, I.; Lloret, F.; Ruiz-García, R.; Julve, M. Molecular magnetism, quo vadis? A historical perspective from a coordination chemist viewpoint. *Coord. Chem. Rev.* **2017**, *339*, 17–103.
20. Martínez-Lillo, J.; Mastropietro, T.F.; Lhotel, E.; Paulsen, C.; Cano, J.; De Munno, G.; Faus, J.; Lloret, F.; Julve, M.; Nellutla, S.; et al. Highly Anisotropic Rhenium(IV) Complexes: New Examples of Mononuclear Single-Molecule Magnets. *J. Am. Chem. Soc.* **2013**, *135*, 13737–13748.
21. Pedersen, K.S.; Sigrist, M.; Sørensen, M.A.; Barra, A.-L.; Weyhermüller, T.; Piligkos, S.; Thuesen, C.A.; Vinum, M.G.; Mutka, H.; Weihe, H.; et al. $[ReF_6]^{2-}$: A Robust Module for the Design of Molecule-Based Magnetic Materials. *Angew. Chem. Int. Ed.* **2014**, *53*, 1351–1354. [CrossRef]
22. Gong, D.-P.; Chen, J.-F.; Zhao, Y.; Cao, D.-K. *Dalton Trans.* **2016**, *45*, 3443–3449.
23. Feng, X.; Liu, J.-L.; Pedersen, K.S.; Nehrkorn, J.; Schnegg, A.; Holldack, K.; Bendix, J.; Sigrist, M.; Mutka, H.; Samohvalov, D.; et al. Multifaceted magnetization dynamics in the mononuclear complex [Re IV Cl 4 (CN) 2] $^{2-}$. *Chem. Commun.* **2016**, *52*, 12905–12908. [CrossRef]
24. Pedersen, K.S.; Bendix, J.; Tressaud, A.; Durand, E.; Weihe, H.; Salman, Z.; Morsing, T.J.; Woodruff, D.N.; Lan, Y.; Wernsdorfer, W.; et al. Iridates from the molecular side. *Nat. Commun.* **2016**, *7*, 12195.
25. Sanchis-Perucho, A.; Martínez-Lillo, J. Ferromagnetic exchange interaction in a new Ir(IV)-Cu(II) chain based on the hexachloroiridate(IV) anion. *Dalton Trans.* **2019**, *48*, 13925–13930. [CrossRef]
26. Su, Q.-Q.; Fan, K.; Huang, X.-D.; Xiang, J.; Cheng, S.-C.; Ko, C.-C.; Zheng, L.M.; Kurmood, M. Field-induced slow magnetic relaxation in low-spin S = 1/2 mononuclear osmium(V) complexes. *Dalton Trans.* **2020**, *49*, 4084–4092. [CrossRef]
27. Woodall, C.H.; Craig, G.A.; Prescimone, A.; Misek, M.; Cano, J.; Faus, J.; Probert, M.R.; Parsons, S.; Moggach, S.; Martínez-Lillo, J.; et al. Pressure induced enhancement of the magnetic ordering temperature in rhenium(IV) monomers. *Nat. Commun.* **2016**, *7*, 13870. [CrossRef]
28. Chiozzone, R.; González, R.; Kremer, C.; De Munno, G.; Cano, J.; Lloret, F.; Julve, M.; Faus, J. Synthesis, Crystal Structure, and Magnetic Properties of Tetraphenylarsonium Tetrachloro(oxalato)rhenate(IV) and Bis(2,2′-bipyridine)tetrachloro(μ-oxalato)copper(II)rhenium(IV). *Inorg. Chem.* **1999**, *38*, 4745–4752. [CrossRef]
29. González, R.; Chiozzone, R.; Kremer, C.; De Munno, G.; Nicolò, F.; Lloret, F.; Julve, M.; Faus, J. Magnetic Studies on Hexaiodorhenate(IV) Salts of Univalent Cations. Spin Canting and Magnetic Ordering in $K_2[ReI_6]$ with T_c = 24 K. *Inorg. Chem.* **2003**, *42*, 2512–2518. [CrossRef]
30. González, R.; Chiozzone, R.; Kremer, C.; Guerra, F.; De Munno, G.; Lloret, F.; Julve, M.; Faus, J. Magnetic Studies on Hexahalorhenate(IV) Salts of Ferrocenium Cations $[Fe(C_5R_5)_2]_2[ReX_6]$ (R = H, CH_3; X = Cl, Br, I). *Inorg. Chem.* **2004**, *43*, 3013–3019. [CrossRef]
31. Martínez-Lillo, J.; Armentano, D.; De Munno, G.; Lloret, F.; Julve, M.; Faus, J. A Two-Dimensional $Re^{IV}Ag^{I}$ Compound: X-ray Structure and Magnetic Properties. *Cryst. Growth Des.* **2006**, *6*, 2204–2206. [CrossRef]
32. Martínez-Lillo, J.; Armentano, D.; De Munno, G.; Marino, N.; Lloret, F.; Julve, M.; Faus, J. A self-assembled tetrameric water cluster stabilized by the hexachlororhenate(IV) anion and diprotonated 2,2′-biimidazole: X-ray structure and magnetic properties. *CrystEngComm* **2008**, *10*, 1284–1287. [CrossRef]
33. Armentano, D.; Martínez-Lillo, J. Hexachlororhenate(IV) salts of ruthenium(III) cations: X-ray structure and magnetic properties. *Inorg. Chim. Acta* **2012**, *380*, 118–124. [CrossRef]

34. Martínez-Lillo, J.; Kong, J.; Julve, M.; Brechin, E.K. Self-Assembly of the Hexabromorhenate(IV) Anion with Protonated Benzotriazoles: X-ray Structure and Magnetic Properties. *Cryst. Growth Des.* **2014**, *14*, 5985–5990. [CrossRef]
35. Martínez-Lillo, J.; Pedersen, A.H.; Faus, J.; Julve, M.; Brechin, E.K. Effect of Protonated Organic Cations and Anion−π Interactions on the Magnetic Behavior of Hexabromorhenate(IV) Salts. *Cryst. Growth Des.* **2015**, *15*, 2598–2601. [CrossRef]
36. Armentano, D.; Martínez-Lillo, J. Aquapentachlororhenate(IV): A singular and promising building block for metal assembly. *RSC Adv.* **2015**, *5*, 54936–54940. [CrossRef]
37. Armentano, D.; Martínez-Lillo, J. Anion-Assisted Crystallization of a Novel Type of Rhenium(IV)-Based Salt. *Cryst. Growth Des.* **2016**, *16*, 1812–1816. [CrossRef]
38. Pedersen, A.H.; Julve, M.; Brechin, E.K.; Martínez-Lillo, J. Self-assembly of the tetrachlorido (oxalato) rhenate (IV) anion with protonated organic cations: X-ray structures and magnetic properties. *CrystEngComm* **2017**, *19*, 503–510. [CrossRef]
39. Pedersen, A.H.; Geoghegan, B.L.; Nichol, G.S.; Lupton, D.W.; Murray, K.S.; Martínez-Lillo, J.; Gass, I.A.; Brechin, E.K. Hexahalorhenate(IV) salts of metal oxazolidine nitroxides. *Dalton Trans.* **2017**, *46*, 5250–5259. [CrossRef]
40. Armentano, D.; Barquero, M.A.; Rojas-Dotti, C.; Moliner, N.; De Munno, G.; Brechin, E.K.; Martínez-Lillo, J. Enhancement of Intermolecular Magnetic Exchange through Halogen Halogen Interactions in Bisadeninium Rhenium(IV) Salts. *Cryst. Growth Des.* **2017**, *17*, 5342–5348. [CrossRef]
41. Rojas-Dotti, C.; Moliner, N.; González, R.; Martínez-Lillo, J. Hexakis(dimethylformamide)iron(II) complex cation in hexahalorhenate(IV)-based salts: Synthesis, X-ray structure and magnetic properties. *J. Coord. Chem.* **2018**, *71*, 737–747. [CrossRef]
42. Armentano, D.; Sanchis-Perucho, A.; Rojas-Dotti, C.; Martínez-Lillo, J. Halogen···halogen interactions in the self-assembly of one-dimensional 2,2′-bipyrimidine-based $Cu^{II}Re^{IV}$ systems. *CrystEngComm* **2018**, *20*, 4575–4581. [CrossRef]
43. Dance, I.; Scudder, M. Supramolecular Motifs: Concerted Multiple Phenyl Embraces between Ph_4P^+ Cations Are Attractive and Ubiquitous. *Chem. Eur. J.* **1996**, *2*, 481–486. [CrossRef] [PubMed]
44. Dance, I.; Scudder, M. Supramolecular motifs: Sextuple aryl embraces in crystalline $[M(2,2'\text{-bipy})_3]$ and related complexes. *J. Chem. Soc. Dalton Trans.* **1998**, 1341–1350. [CrossRef]
45. Orts-Arroyo, M.; Castro, I.; Lloret, F.; Martínez-Lillo, J. Molecular Self-Assembly in a Family of Oxo-Bridged Dinuclear Ruthenium(IV) Systems. *Cryst. Growth Des.* **2020**, *20*, 2044–2056. [CrossRef]
46. Bain, G.A.; Berry, J.F. Diamagnetic Corrections and Pascal's Constants. *J. Chem. Educ.* **2008**, *85*, 532–536. [CrossRef]
47. SAINT. *Bruker Analytical X-ray Systems*; Version 6.45; SAINT: Madison, WI, USA, 2003.
48. Krause, L.; Herbst-Irmer, R.; Sheldrick, G.M.; Stalke, D. Comparison of silver and molybdenum microfocus X-ray sources for single-crystal structure determination. *J. Appl.Cryst.* **2015**, *48*, 3–10. [CrossRef]
49. Sheldrick, G.M. Crystal structure refinement with SHELXL. *Acta Cryst.* **2015**, *C71*, 3–8.
50. Sheldrick, G.M. A short history of SHELX. *Acta Cryst.* **2008**, *A64*, 112–122. [CrossRef]
51. SHELXTL-2013/4. *Structure Determination Software Programs*; Bruker Analytical X-ray Instruments Inc.: Madison, WI, USA, 2013.
52. DIAMOND 4.5.0. *Crystal Impact GbR, Crystal Impact*; Brandenburg GbR, Kreuzherrenstr: Bonn, Germany, 2018.